Zoosyst. Evol. 94 (1) 2018, 195–209 | DOI 10.3897/zse.94.22289

PENSOFT

museum für naturkunde

Ontogeny of *Hemidactylus* (Gekkota, Squamata) with emphasis on the limbs

Wessel van der Vos[1], Koen Stein[2,3], Nicolas Di-Poï[4], Constanze Bickelmann[1]

1 *Museum für Naturkunde Berlin, Leibniz Institute for Evolution and Biodiversity Science, Invalidenstrasse 43, 10115 Berlin, Germany*
2 *Earth System Science – AMGC, Vrije Universiteit Brussel, Pleinlaan 2, 1050 Brussels, Belgium*
3 *Royal Belgian Institute of Natural Sciences, Earth and History of Life, Rue Vautier 29, 1000 Brussels, Belgium*
4 *Institute of Biotechnology, Research Program in Developmental Biology, University of Helsinki, Finland*

http://zoobank.org/122E692A-9E01-47FB-A386-D4E707620460

Corresponding author: *Constanze Bickelmann* (constanze.bickelmann@mfn.berlin)

Received 15 November 2017
Accepted 12 February 2018
Published 9 March 2018

Academic editor:
Johannes Penner

Key Words

Gecko
in-ovo development
staging table
limb development
bone histology
μCT
immunohistochemistry
ossification
ecomorphological specialization

Abstract

Squamate reptiles constitute a major component of the world's terrestrial vertebrate diversity, encompassing many morphotypes related to ecological specialization. Specifically, Gekkota, the sister clade to most other squamates, have highly specialized autopodia, which have been linked to their ecological plasticity. In this study, a developmental staging table of the gecko *Hemidactylus*, housed at the Museum für Naturkunde, is established. Twelve post-ovipositional stages are erected, monitoring morphological embryological transitions in eye, ear, nose, heart, limbs, pharyngeal arches, and skin structures. Ecomorphological specializations in the limbs include multiple paraphalanges, hypothesized to aid in supporting the strong muscles, that are situated adjacent to metacarpal and phalangeal heads. Furthermore, some phalanges are highly reduced in manual digits III and IV and pedal digits III, IV, and V. Development, composition, and growth of limb elements is characterized in detail via μCT, histochemistry, and bone histological analysis. Using known life history data from two individuals, we found an average lamellar bone accretion rate in the humeral diaphysis comparable to that of varanids. Various adult individuals also showed moderate to extensive remodeling features in their long bone cortices, indicating that these animals experience a highly dynamic bone homeostasis during their growth, similar to some other medium-sized to large squamates. This study of *in-ovo* development of the gecko *Hemidactylus* and its ecomorphological specializations in the adult autopodia, enlarges our knowledge of morphological trait evolution and of limb diversity within the vertebrate phylum.

Introduction

Gekkota (Squamata; lizards, snakes and amphisbaenians *sensu* Wiens et al. 2012) is a speciose and ecologically diverse clade with a cosmopolitan distribution (Carranza and Arnold 2006). Yet, molecular and morphological data for squamate interrelationships disagree substantially (Losos et al. 2012); however, according to the molecular data, Gekkota are, together with Dibamidae, sister to all other squamates (Wiens et al. 2012, Pyron et al. 2013). Although squamate reptiles contribute greatly to vertebrate diversity in modern ecosystems, and exhibit a wide range of morphological variation in their limbs related to ecological specialization, underlying developmental and molecular mechanisms remain yet poorly studied (Sanger 2012, Pyron et al. 2013). However, importantly, the incorporation of taxa from all higher clades in the study of development and molecules is essential for understanding evolutionary patterns of development (Millinkovitch and Tzika 2007, Sanger 2012).

Some gekkotan species have the extraordinary ability of being able to cling to smooth surfaces and of inverted locomotion because of the properties of their specialized autopodia (Autumn et al. 2002, Russell 2002, Pianka and Sweet 2005). Such ability is associated with adhesive toepads which are located ventrally on the distal part of the digits (Ruibal and Ernst 1965, Russell 2002, Gamble et al. 2012). In Gekkota, adhesive toepads have first been reported in fossils from Lower Cretaceous amber deposits of Myanmar (Arnold and Poinar 2008). They evolved and were lost independently several times within this lineage, and allowed them to enter novel ecological habitats (Pianka and Sweet 2005, Gamble et al. 2012). Further eco-specializations in Gekkota include the presence of paraphalanges, unique structures only found in the gekkotan clade and hypothesized to aid both in the attachment of strong muscles in the digits and in the grasping power of the limb by applying pressure to the adhesive toepads (Russell and Bauer 1988). These apomorphic elements are located laterally to the interphalangeal joints and occasionally on the dorsal and ventral sides, and vary in number, shape and size (Wellborn 1933, Russell and Bauer 1988, Gamble et al. 2012). Paraphalanges are either cartilaginous or bony structures (Wellborn 1933, Russell and Bauer 1988, Gamble et al. 2012). Paraphalanges have been correlated with functional demands, such as grasping and/or climbing, rather than phylogeny (Russell and Bauer 1988, Vickaryous and Olson 2007, Gamble et al. 2012). They have evolved and were lost multiple times within Gekkota (Gamble et al. 2012).

Besides these general gekkotan traits, one gekkotan genus shows additional ecomorphological specializations in both fore- and hind limbs: *Hemidactylus* (Fig. 1). It is placed within Gekkonidae, as sister to *Cyrtodactylus* (Pyron et al. 2013). It has highly reduced phalanges (Russell 1975, 1977, Gamble et al. 2012). More specifically, the antepenultimate phalanx is highly reduced in digits III and IV of the manus, with a phalangeal count of 2-3-4-5-3 (Russell 1975, 1977). The pes shows a phalangeal count of 2-3-4-5-4, with an additional reduced phalanx in digit V (Russell 1975, 1977). Although phalangeal elements are also reduced in other geckos, the degree of reduction is never as pronounced as in *Hemidactylus* (Gamble et al. 2012).

Here, we present a morphological staging table for *Hemidactylus* based on external embryonic developmental traits and compare these to other squamate taxa. We make further references to characterize limbs which display ecomorphological specializations, and which we study using different approaches such as bone histology, μCT, and immunohistochemistry. Enlarging the database of well documented developmental character traits of organisms allows for a more detailed and comprehensive knowledge of vertebrate morphological diversity. The described ecomorphological specializations in the autopodia of the adult phenotype make *Hemidactylus* an ideal candidate for eco-evo-devo studies (Gilbert and Epel 2009).

Material and methods

Institutional abbreviations

AC – Comparative Anatomy, Musée d'Histoire Naturelle, Paris, France; CA – Cold Archive, Museum für Naturkunde Berlin, Leibniz Institute for Evolution and Biodiversity Science, Berlin, Germany; MK – Museum Koenig, Bonn, Germany; ZMB – Museum für Naturkunde Berlin, Leibniz Institute for Evolution and Biodiversity Science (former Zoologisches Museum Berlin), Berlin, Germany.

Figure 1. An adult *Hemidactylus* female (three years old).

Animal care

The study organism *Hemidactylus* is a yet unidentified species based on a pregnant female which was collected in Sudan in 2011 (Fig. 1; ZMB 87075 to 87077; Kirchhof et al. work in progress). Live animals are housed in an animal-care facility at the Museum für Naturkunde Berlin; dead animals are preserved in alcohol in the herpetological collection and the Cold Archive at the Museum für Naturkunde Berlin. Temperature in the breeding room is set to 26-28 °C and photoperiod is maintained at 12 hours daylight: 12 hours of darkness. Seasonal cycles are not mimicked. Animals are fed with house crickets (*Acheta domesticus*), fruits, vitamins and calcium powder twice weekly. Females are allowed to oviposit naturally. Eggs are laid in clutches of one to two. Duration of post-ovipositional development is approximately 60 days, comparable to that of the Madagascar Ground Gecko *Paroedura pictus* (Noro et al. 2009). Embryos were sacrificed in accordance with German Law on *Tierschutzgesetz*, and *TierSchVersV*. Embryos were fixed in 4 % pFA in 1X Phosphate buffered saline (PBS) for 24 h to 48 h, depending on size, dehydrated and stored in 100 % methanol at -20 °C in the Cold Archive at the Museum für Naturkunde Berlin (Tab. 1).

μCT analysis

μCT scans were performed using a Phoenix nanotom X-ray|s at the Museum für Naturkunde Berlin (Suppl. material 1: SOM Tab. 1). Scans were reconstructed to a 3D volume using datos|x (Version 2.0, GE Sensing & Inspection Technologies GmbH phoenix|x-ray). Data were analyzed and visualized with VolumeGraphics Studio Max (Version 2.2., Volume Graphics). Scanned hands were from an adult specimen (Fig. 2; ZMB 87075, SVL 42 mm, over one year old), and a juvenile (Fig. 5C; ZMB 87077, SVL 17 mm, two days old). Datasets and models are deposited here https://doi.org/10.7479/qs1j-mnjp.

Bone Histology

We used two histo-technological procedures: (i) azan stained microtome paraffin sections and (ii) ground petrographic sections.

For azan staining, limbs were embedded (Leica EG 1160 and Shandon Hypercenter XP) in paraffin, and sectioned with a microtome (Leica 2000R). Sections were treated following the standard protocol by Heidenhain. In detail, sections were washed or immersed in xylene paraffin (ten minutes), xylene (twice five minutes), aniline alcohol (five minutes), wash in aquadest, azocarmine (25 minutes), wash in aquadest, wash in acetic acid, and 5 % phosphotungstic acid (two times 20 seconds), one to three hours in 5 % phosphotungstic acid. Hereafter, the tissue was placed in the aniline blue orange dye (4.5 minutes), washed with aquadest, 96 % alcohol, absolute alcohol, and finally four times xylene for five minutes each. Azan stains both bone and cartilage: dark blue indicates bone and light blue cartilage. Red indicates muscle fibers, and the nuclei are stained dark red. A forelimb of a hatchling (Fig. 5A; cross section no. A5_F_13a, specimen ZMB 87077) and a juvenile (Fig. 5B; cross section no. A4_F_21a, specimen ZMB 87076, SVL 33 mm, one year old), and an adult (Fig. 6B, D, E; ZMB 87078, SVL 47 mm, over one year old) were embedded in paraffin and sectioned. Cross sections are stored at the Museum für Naturkunde Berlin.

For ground sections (Fig. 6A, C), macerated bones were dehydrated in 70 % alcohol for 48 hours and embedded in epoxy resin (Araldite 2020), cut along the desired surface, mounted on glass slides and ground to a thickness of 75 to 50 μm. To enhance contrast, prevent detachment due to rehydration and generally protect the section, a coverslip was added. Femoral sections of *Iguana iguana* (AC1896 288), *Varanus timorensis* (MK52920) and *Tupinambis teguixin* (MK53531) were studied at the histotheca facilities of the Museum d'Histoire Naturell in Paris.

Morphometry

Photographs of embryos were taken with a Leica M205C camera. Photomicrographs for histomorphometric analysis of lamellar bone apposition rates were taken on a Zeiss Axioskop (HBO 50) with Leica firecam (DFC 420) and processed in a Leica Application Suite. All measurements were taken using ImageJ (Rasband 1997) (Tabs 1, 2).

Table 1. Developmental age range and external length measurements of *Hemidactylus* stages A to L. All embryos were studied to identify key features characteristic for each stage.

Stage	Developmental days post oviposition	Snout vent length (range in mm)	Forelimb measurement (mean in mm)	Hind limb measurement (mean in mm)	Number of studied specimens
A	4–5	9.3–11.5	n/a	n/a	3
B	6	17.4–20.1	0.2	0.3	2
C	9–14	14.1–17.6	0.7	0.6	4
D	11–30	18.9–24.7	1.5	1.4	11
E	8–30	21.0–24.0	1.8	1.8	7
F	42–56	23.8–24.0	2.8	2.8	2
G	15–36	23.8–27.2	2.8	2.8	6
H	38–50	26.4–31.1	3.7	3.5	6
I	35–56	29.0–34.2	4.9	4.8	10
J	40	32.8–34.2	5.3	6.5	2
K	40–58	36.0–39.4	6.2	6.7	3
L	50–60	37.5–41.9	6.8	6.9	2

Table 2. Histomorphometric data obtained from humeri of an adult (ZMB 87078) and a 'stage I' (CA2017_014). These data were used to calculate average apposition and lamellar bone accretion rates.

	Humerus ZMB 87078		Humerus CA2017_014
Life history data	Adult, Born 10.12.15, deceased 22.03.17		Stage I development
Total days lived	468		25 (unborn)
Days since onset ossification	493		0
Humerus shaft width (µm)	587.6		161.0
	posterior cortex	anterior cortex	
Non-remodeled Cortical thickness (µm)	139.4	91.2	0.1
No. of lamellae in cortex	40	29	1

Immunohistochemistry

Immunohistochemistry was performed on sections, with a rabbit polyclonal anti-*Sox9* antibody (Merck Millipore). *SOX9* is an early marker of cartilage, tendons and ligaments (Sugimoto et al. 2013). Samples were deparaffinized in xylene and rehydrated through ethanol steps into 1X PBS. Antigen retrieval was accomplished by citrate buffer treatment (pH = 6.0). Protease XXV treatment (Thermo Scientific) for 15 min was followed by non-specific binding with 5 % goat serum (Sigma). Primary antibody (polyclonal, rabbit, Millipore) was incubated overnight. Staining was achieved by DAPI and Fluoroshield (Sigma).

Results

Morphological staging table

A morphological staging table of *Hemidactylus* establishing twelve post-ovipositional developmental stages is presented here (Figs 2, 3; Tab. 1). For this purpose, differences in pharyngeal arches, otic pit, olfactory pit, optic cup, and other characters are studied in detail. In the following, each stage is presented listing key features which have been established in other squamate staging tables and which have been considered suitable for characterizing the ontogenetic development (Tab. 3; e.g. Noro et al. 2009, Wise et al. 2009, Khannoon 2015).

Stage A

Ear: The otic pit is present and located dorsally to the hyoid arch (Fig. 2A, B). The cartilage capsule lies dorsally to the otic pit (Fig. 2B).

Eye: The eye is composed of an optic cup that has not yet fully enclosed the lens (Fig. 2A).

Heart: The heart shows the distinct s-shape resulting from the curvature of the developing ventricle. It protrudes from the thoracic cavity.

Nose: The snout starts to form at the rostral end of the head. The olfactory pit is visible as a sickle shaped rim with its curvature pointing to the cranial side and the two points of the rim facing ventrally, towards the heart (Fig. 2B). Between the anterior ends of the rim towards the middle of the dorsal end of the rim, there is a small membrane covering the pit.

Pharyngeal arches: The mandibular pharyngeal arch is prominent, with a small bud from the maxillary that has just started to bud out (Fig. 2A). Posterior to the mandibular pharyngeal arch, the hyoid arch is present. It slightly overlaps the mandibular arch ventrally at the proximal part. Ventral to the hyoid arch is a small slit, marking the future distinction between the hyoid arch and the third arch.

Stage B

Ear: The cartilage capsule dorsal to the otic pit is enlarged (Fig. 2C).

Eye: The optic cup has almost enclosed the lens, except for a small gap rostro-ventrally. Note that this is not the characteristic choroid fissure. The optic cup shows faint pigmentation at the caudal-dorsal margin (Fig. 2D).

Head: The mesencephalon protrudes prominently in the cranial direction.

Heart: The heart and its placement in the thoracic cavity have not changed in comparison to the previous stage (Fig. 2D).

Limbs: Both fore- and hind limbs appear as small buds (Fig. 2C).

Nose: The rim of the olfactory pit is still partially covered by a membrane.

Pharyngeal arches: The maxillary process has not proceeded its development compared to the previous stage. The mandibular and hyoid arches, including the gap between them (Fig. 2D; indicated by the plus), have increased in size and show a sharper medial turn at their distal ends, and the segregation of the ventral part of the hyoid arch is more distinct than in the previous stage (Fig. 2D). The fourth arch and the associated pharyngeal slit are present posterior to the hyoid arch (Fig. 2C; indicated by the asterisk).

Stage C

Ear: The otic pit is enlarged and extends antero-posteriorly beyond the mandibular and hyoid arches. There is less overlap with the cartilage capsule.

Eye: The eye is enlarged and pigmented; it is referred to as the retina pigmented epithelium. The choroid fissure is present, and an unpigmented caudal-rostral line divides the optic cup into a distal and a proximal part (Fig. 2E, F; indicated by the cross).

Limbs: Both limb buds are proximo-distally longer than wide. The apical ectodermal ridge (AER) is distinct (Fig. 2G).

Nose: The external nares have developed, replacing the olfactory pit (Fig. 2E, F). This process of the fronto-nasal process replaces the olfactory rim. The dorsal side of the covering membrane is now connected to the maxillary process.

Pharyngeal arches: The maxillary process is linked to the dorsal side of the fronto-nasal process. The mandibu-

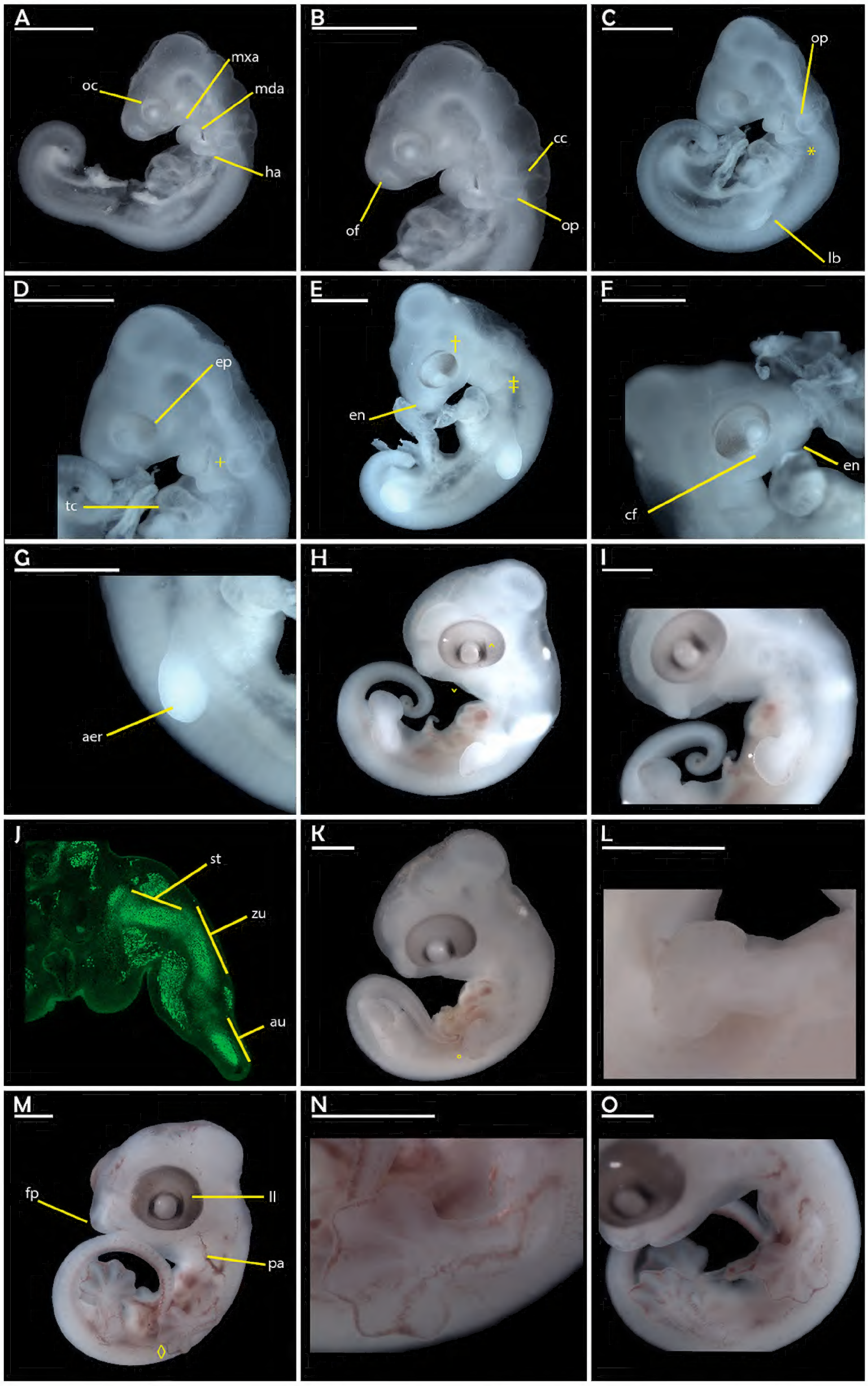

Figure 2. Overview of embryonic developmental stages A to F, erected in this study. Stage A is depicted in **(A, B)** and represented by CA2017_007. **(C, D)** show the representative CA2017_003 for stage B. Stage C **(E–G)** is represented by CA2017_006. CA2017_005 represents stage D in **(H–J)**. Note the immunohistochemistry for *SOX9* expression in a limb cross section in **(J)**. Stage E is shown in **(K–L)**, represented by CA2017_010. CA2017_012 represents stage F in **(M-O)**. Except for **(J)**, all pictures in lateral view. Scale bars equal 1mm. Abbreviations: **aer** – apical ectodermal ridge; **au** – autopod; **cc** – cartilage capsule; **cf** – choroid fissure; **en** – external nares; **ep** – eye pigmentation; **fp** – frontal nasal process; **ha** – hyoid arch; **lb** – limb bud; **ll** – lateral lines; **mda** – mandibular arch; **mxa** – maxillary process; **oc** – optic cup; **of** – olfactory pit; **op** – otic pit; **pa** – pharyngeal arches; **st** – stylopod; **tc** – thorac cavity; **zu** – zeugopod.

lar arch has budded out. The slit between the mandibular and the hyoid arch is reduced. The fourth and the fifth arches are present as small buds (Fig. 2E; indicated by the double-cross).

Stage D

Ear: The otic vesicle is less prominent in comparison to former stages.

Eye: The eye displays darker pigmentation, including its extension rostrally and caudally to the lens (Fig. 2H; indicated by the upside caret), which is here interpreted as the precursor of the iris.

Heart: The heart is fully enclosed inside the thoracic cavity.

Limbs: Fore- and hind limbs show the paddle shape typically seen in other amniote embryos at corresponding stages (Fig. 2H, I). An elbow angle between the stylopod and zeugopod starts developing. *SOX9*, the precursor of cartilage, is expressed in the presumptive stylopod, zeugopod, and autopod regions (Fig. 2J). Expression is also distinct in the presumptive regions of the strong limb muscles (Fig. 2J).

Nose: The rim of the olfactory pit is completely closed. The maxillary and the medial nasal prominence overlay the stomodeum.

Pharyngeal arches: The mandibular arch and the hyoid arch are now indistinguishable from one another (Fig. 2H; indicated by the downside caret), and the fourth arch has begun to grow, becoming larger than the initial bud. The mandibular arch reaches to the midline of the eye, and the maxillary prominence has taken up a position anterior to the eye.

Stage E

Ear: The otic vesicle further extends over the length of the mandibular and hyoid arch.

Eye: Lines that are visible lateral to the eye, or primordial iris, flanking the lens, have differentiated further.

Limbs: The most pronounced differences between stages D and E are identifiable in the limbs. In both fore- and hind limb, the interdigital tissue is retreating (Fig. 2K, L; indicated by the circle). A blood vessel is present at the distal margin of the forming autopod, which is antero-posteriorly wider than it is proximo-distally long (Fig. 2K).

Nose: Deep furrows between the nasal and maxillary prominences are developing further and show invaginations in this region.

Pharyngeal arches: The prominence of the mandibular and hyoid arches is now located anterior to the lens.

Stage F

Ear: The otic capsule has now become a small pit on the lateral side of the head.

Eye: The optic cup is darkly pigmented. The lateral pigmented lines now enclose the lens (Fig. 2M).

Limbs: Recession of the interdigital tissue is extensive (Fig. 3M-O; indicated by the rhomb). The autopodia have increased in size, most notably across the antero-posterior axis (Fig. 2N).

Nose: The olfactory pit has disappeared. The fronto-nasal process is fully fused (Fig. 3M).

Pharyngeal arches: The pharyngeal arches do not show the distinction between the different arches anymore (Fig. 2M).

Stage G

Ear: No further development in comparison to the former stage (Fig. 3A).

Eye: The optic cup has completely encircled the lens. The lateral pigmented lines of the lens start to encircle the lens and intensify in pigmentation.

Head: Cephalic projections, except for the mesencephalon, have disappeared. The head resembles that of a hatchling. Internally, only the calcified endolymphatic sacs and statolithic masses are visible in the μCT scans (Fig. 3B).

Limbs: The autopodia show further recession of the interdigital tissue, prominently segregating digits I to V. The elbow angle is at 90°. First signs of slightly swollen patches on the ventral side of the digits are visible (Fig. 3C).

Nose: The nose has become a pit laterally at the rostral end of the snout (Fig. 3A).

Jaw: Upper and lower jaws are fully formed.

Urogenital bud: The urogenital bud is located medially between the hind limbs (Fig. 3A).

Stage H

Eye: There are four distinct changes that are present in the eye at this stage: (i) The lens has changed from a matte white color to a more shining white color. (ii) The iris starts to cover the margins of the lens. (iii) The black pigmented tissue, starting out as the optic cup, has a glassy appearance. (iv) The hollow pan surrounding the lens is lighter than the rest of the eyeball.

Head: The head surface is smooth with few irregularities. The mesencephalon is still identifiable. Skull bones, such as parietal and surangular, start ossifying (Fig. 3E).

Limbs: The digits are almost free of interdigital tissue, and the distal phalanges start showing claw formation (Fig. 3D, F). Limb elements are still cartilaginous (Fig. 3E). On the ventral side of the digits, swollen pads are distinct, representing the precursors of the adhesive toepads (Fig. 3D, F).

Stage I

Eye: The iris surrounding the lens starts to display a wavy pattern but is still confined along the margin (Fig. 3G).

Head: More or less all skull bones are ossifyed (Fig. 3H).

Limbs: Claws have developed on all digits. Adhesive toepads are more prominent at this stage: one can discriminate the wavy skin and swellings on the toepads (Fig. 3I). All long bones have started ossifying, as well as the metacarpals in the forelimbs (Fig. 3H). In the hind limbs, metatarsals have ossified further compared to the forelimbs, and ossification of the proximal phalanges has just set in (Fig. 3H).

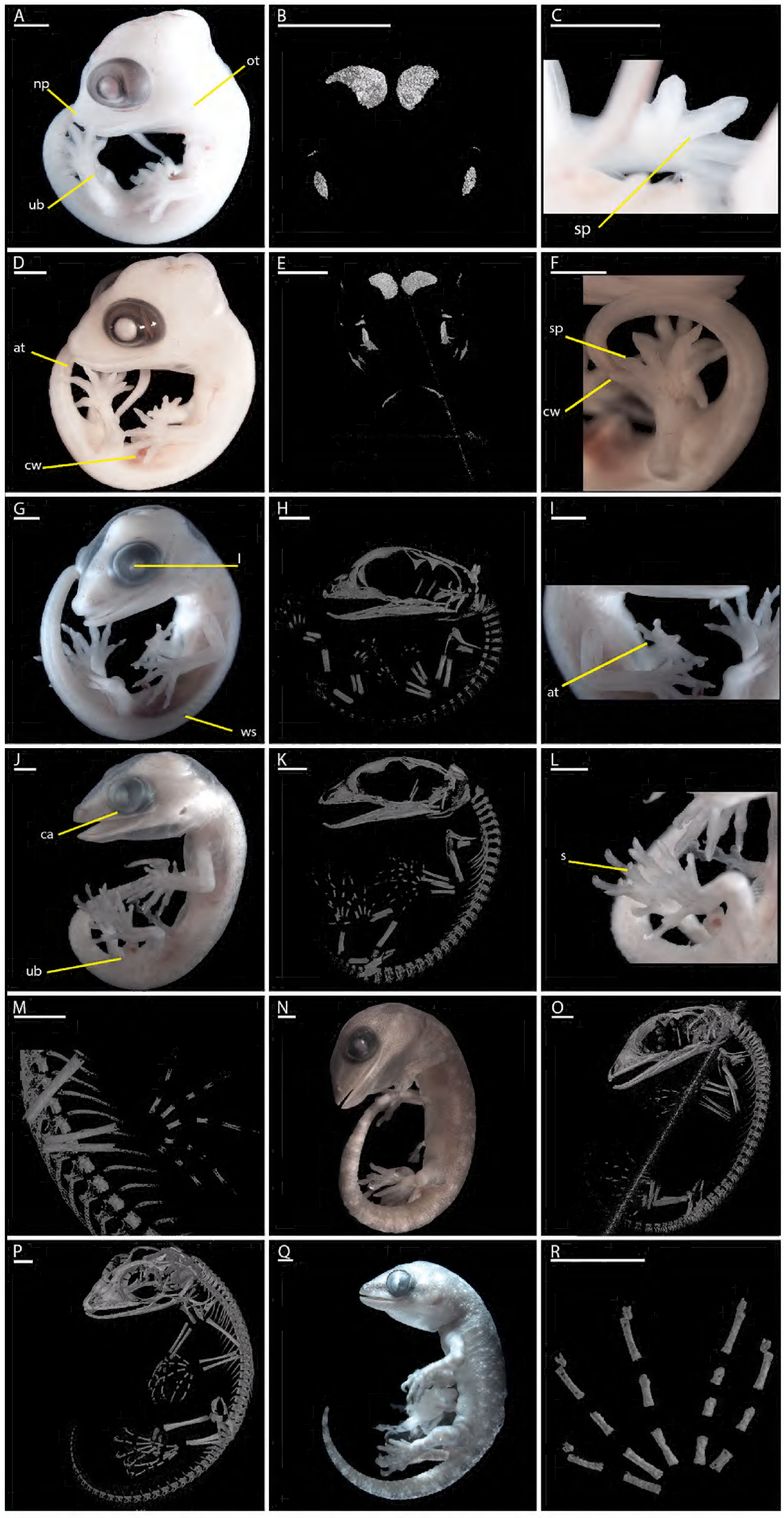

Figure 3. Overview of embryonic developmental stages G to L, erected in this study, including μCT data. Stage G is shown in **(A–C)**, its representative is CA2017_004. CA2017_011 represents stage H in **(D–F)**. **(G–I)** show stage I represented by CA2017_014. Stage J is depicted in **(J–M)**, represented by CA2017_008. Stage K is CA2017_013 and shown in **(N, O)**. **(P–R)** show CA2017_002 for stage L. **(B)** and **(E)** are in cranial view, **(R)** in dorsal view, and all others in lateral view. Scale bars equal 1mm. Abbreviations: **at** – adhesive toepads; **ca** – cornea; **cw** – claw formation; **l** – lens; **np** – nose pit; **ot** – otic capsule; **s** – scansors; **sp** – swollen pads; **ub** – urogenital bud; **ws** – wrinkly skin.

Skin: The skin starts to get wrinkly, a precursor stage prior to scale formation of the skin (Fig. 3G). Scale formation starts on the tail and proceeds cranially.

Stage J

Eye: Within the eye, the cornea is developing, and the eye socket begins to enclose the eye (Fig. 3J). The iris has a distinct shape, with projections pointing to the medial part of the lens.

Head: The mesencephalon has started to retract, exposing a smooth skull.

Limbs: The limbs are fully developed. Even the scales, although not yet fully pigmented, are present on the limbs. The scansors on the ventral adhesive toepads of the digits now show a rough wavy texture (Fig. 3L). The most distal part of the adhesive toepads no longer connects dorsally to the ventral part of each digit. All phalangeal elements have started ossifying (Fig. 3K, M).

Nose: The nose has moved to the most rostral side of the snout; it will not change position hereafter.

Skin: Scales now cover the entire body. The skin is dark.

Urogenital bud: The urogenital bud has started retreating into the body (Fig. 3J).

Stage K

Eye: The eye is located inside the socket, and the scale ridge surrounding it starts to develop (Fig. 3N). The scleral plates of the sclerotic ring start ossifying (Fig. 3O).

Head: Fully scaled.

Limbs: Ossification of the long bones continues (Fig. 3O).

Skin: All scales are pigmented. Scales are present on the upper and lower jaw.

Stage L

Eye: There is a rim on the cranial side of the eye, starting dorsally and wrapping around the upper part of the socket all the way to the midline (Fig. 3Q). The sclerotic ring is fully ossified (Fig. 3P).

Limbs: Phalanges and metacarpals and -tarsals continue ossifying, with the epiphyses not yet being ossified (Fig. 3R). Yet, neither paraphalanges nor carpals or tarsals have started ossifying (Fig. 3R).

Skin: The scales, present on tail, back, limbs, and head show differences in pigmentation and color (Fig. 3Q).

Limb ossification

The phenomenon of limb reduction is of great interest in evolutionary biology (e.g. Shapiro 2002), and especially among squamates, it is frequently found and has been linked to functional demands. Among the many mechanisms and patterns observed that go hand in hand with limb reduction, skeletal heterochrony can be one of them (Shapiro 2002, Hugi et al. 2012). *Hemidactylus* has reduced phalangeal elements, which could represent an evolutionary step along the path of digit loss (Hopson 1995). In that regard, we analysed limb ossification in *Hemidactylus* limbs.

Between fore- and hind limbs, no heterochronic differences in size and shape were monitored at any developmental stage (Figs 2, 3; Tab. 1). Ossification sets in slightly earlier in hind autopodial elements compared to the forelimb ones (Fig. 3H). Reduced phalanges ossify at the same time and in the same order as other phalanges (Fig. 3).

Histochemical staining and μCT scanning show that the paraphalangeal elements of *Hemidactylus* are present in three different shapes (Figs 4, 5): (i) nubbin-like ones laterally and dorsally at the distal end of all metacarpals, as well as at the dorsal side at the distal end of each last phalanx (Fig. 4; labeled in orange); (ii) rhomb-shaped ones distal-lateral to phalanx 1 in digits II, III, IV, and V, as well as phalanx 2 in digit IV (Fig. 4; labeled in red); and (iii) oval paraphalanges located ventrally at metacarpal heads of digits II to V (Fig. 4; labeled in yellow). All paraphalanges are bony in one-year-old adults (ZMB 87075, ZMB 87076) (Fig. 4, 5B). Yet, ossification starts only after hatching; in the two-day-old specimen (ZMB 87077) it has not yet started.

Long bone histology and histomorphometry

The long bones of one-year-old adult individuals show a lamellar bone matrix with no vascular spaces (Fig. 6). Growth lines may sometimes be present in the primary cortex of individuals over one year old, but in some individuals they are absent or have been resorbed by medullary expansion. These individuals also show intense endosteal remodelling features in the diaphyseal cortex, as seen in longitudinal section (Fig. 6A, B). Different generations of resorption and redeposition of endosteal bone can be seen along the margin of the innermost cortex, expressed by the cross-cutting relations of the resorption lines. Such remodeling features in the endosteal region can also be observed in other lizard species, such as varanid, tegu and iguanid lizards (Fig. 7), but only *Tupinambis* shows true secondary osteons in the innermost cortex among sampled squamates.

From an adult individual of known age (ZMB 87078, 468 days old, 493 days since onset of ossification, Fig. 6B, D, E; Tab. 2), we calculated the average daily lamellar bone apposition rate since the onset of ossification until time of death at 0.1 lamellae per day, equivalent to an average periosteal accretion rate of 0.4 μm per day. We used the following formulae to calculate accretion rates:

$$Average[apposition.rate] = \left(\frac{W_{adult.hum} - W_{onset.oss}}{2}\right) \times \left(\frac{1}{N°_{days.onset.oss}}\right)$$

$$Average[lamellar.accretion.rate] \left(\frac{W_{adult.hum} - W_{onset.oss}}{}\right) \times \left(\frac{1}{N_{\ days\ onset\ oss}}\right) \times \left(\frac{N°_{lamellae.primcortex}}{W_{primcortex}}\right)$$

Where apposition.rate is the daily accretion rate (in μm/day), lamellar.accretion.rate is the number of lamellae deposited per day, $W_{adult.hum}$ is the width of the adult humerus (in μm), $W_{onset.oss}$ is the humeral width at the onset of ossification (in μm), $N°_{days.onset.oss}$ is the age of the adult individuals, in days, since the onset of ossification, $W_{primcortex}$ is the thickness of the primary cortex in the adult individual, and $N°_{lamellae.primcortex}$ is the number of lamellae counted in the primary cortex of the adult individual (Measurements in Tab. 2).

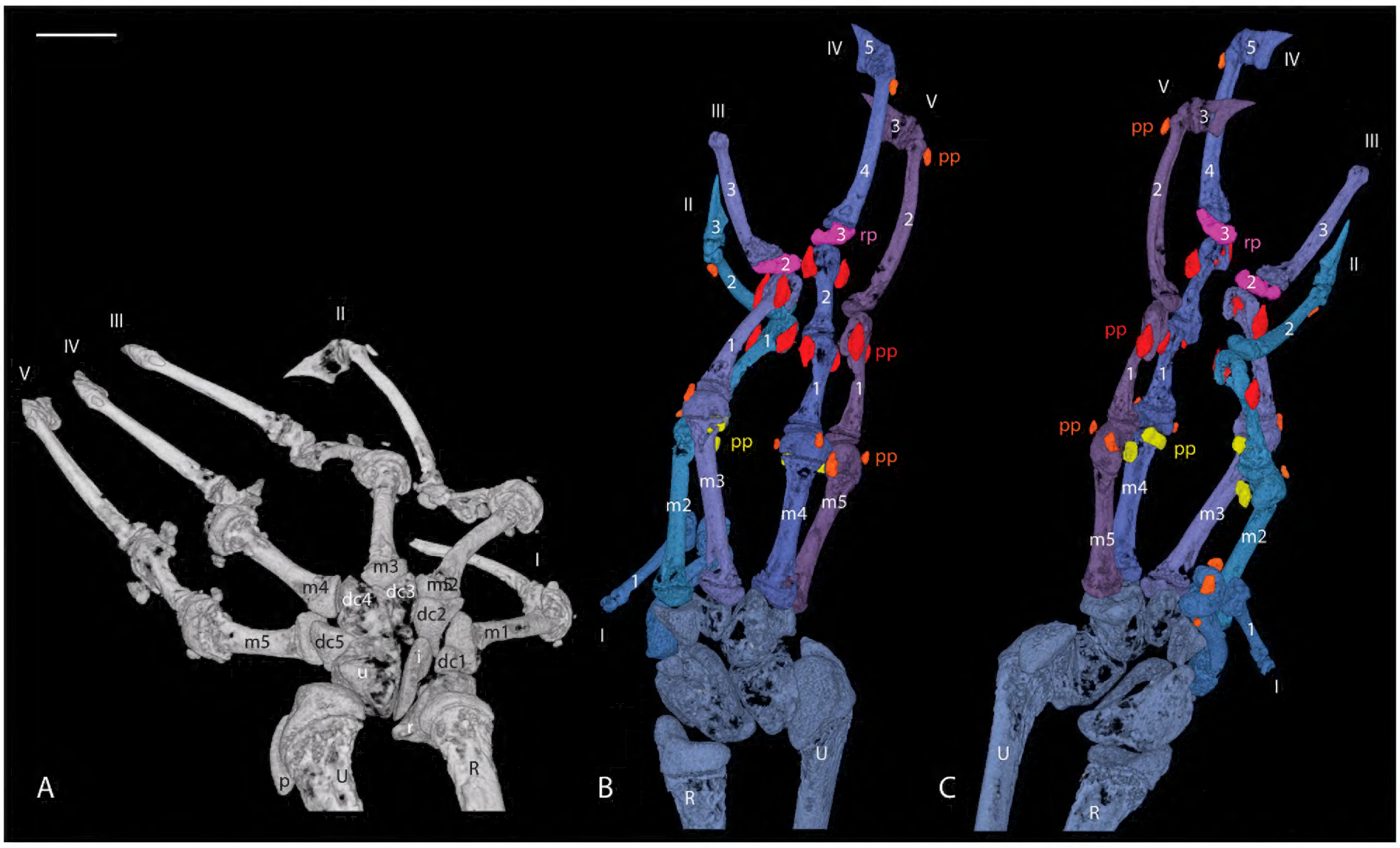

Figure 4. μCT images of the manus of an adult *Hemidactylus* (ZMB 87075). Left **(A)** and right **(B, C)** manus in dorsal **(A, B)** and ventral **(C)** view. Large lateral paraphalanges are shown in red, small nubbin-like ones laterally and dorsally in orange, and ventral ones in yellow. Note the reduced antepenultimate in pink in **(B, C)**. Scale bar is 500 μm. Abbreviations: **dc** – distal carpals; **m** – metacarpals; **p** –pisiform; **pp** – paraphalanges; **R** – radius; **r** – radiale; **rp** – reduced phalanges; **U** – ulna; **u** – ulnare; **1-5** – phalanges 1-5; **I-V** – digits I-V.

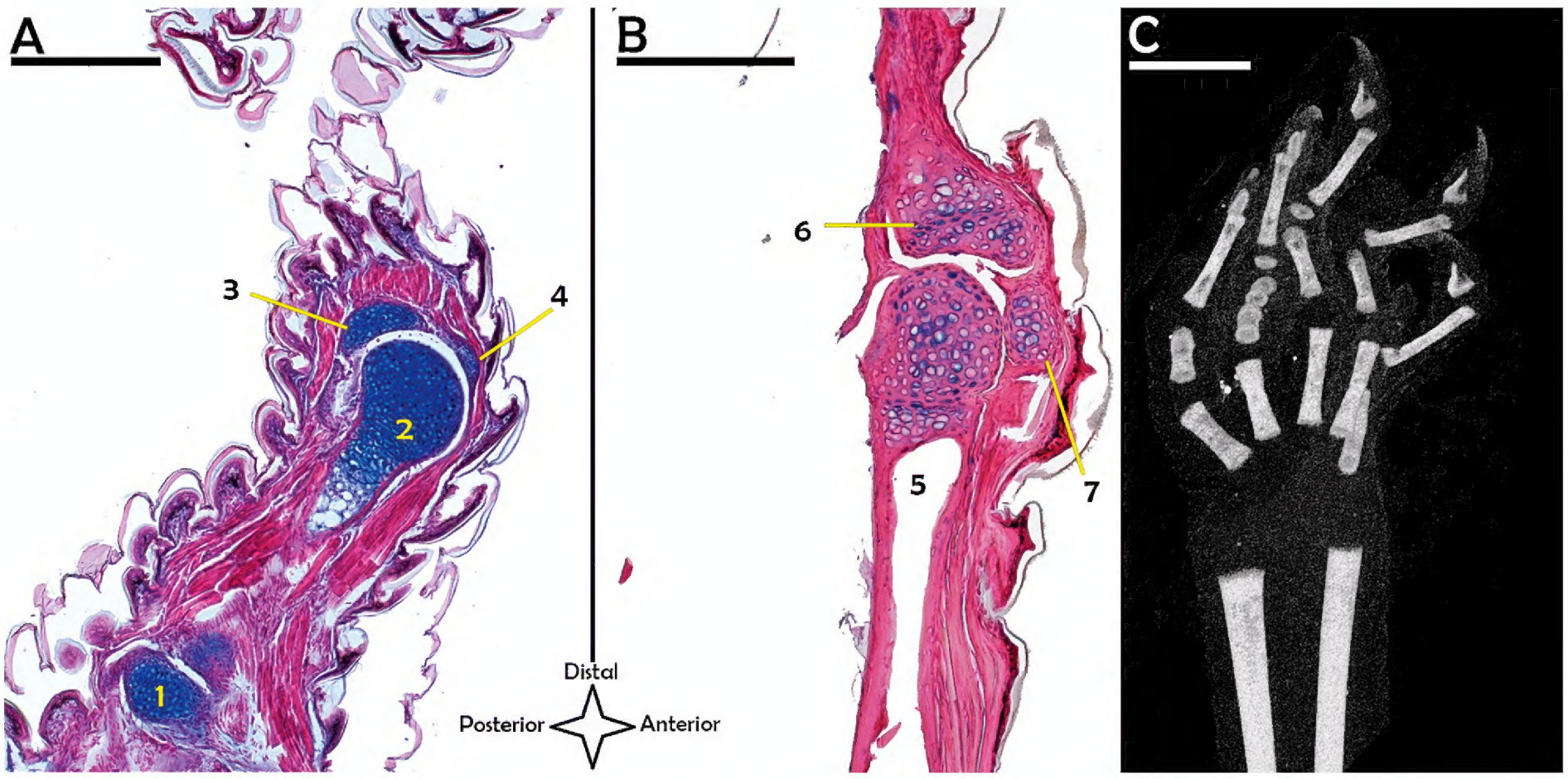

Figure 5. Forelimb of juvenile *Hemidactylus*, stained with azan **(A, B)** and scanned by μCT **(C)**. **(A)** and **(C)** are of the hatchling ZMB 87077 (cross section no. in A is A5_F_13a), and **(B)** of the juvenile ZMB 87076 (cross section no. A4_F_21a). Note the yet unossified paraphalanges in both. In contrast, reduced phalangeal elements have started ossifying. Radius and ulna are not yet fully ossified, and carpal elements are as yet unossified. Numericals indicate: **1** – trapezium; **2** – metacarpal; **3** – phalanx; **4** – paraphalanx; **5** – metacarpal; **6** – phalanx; **7** – paraphalanx. Scale bars in **(A)** and **(B)** equal 200 μm, and scale bar in **(C)** is 550 μm.

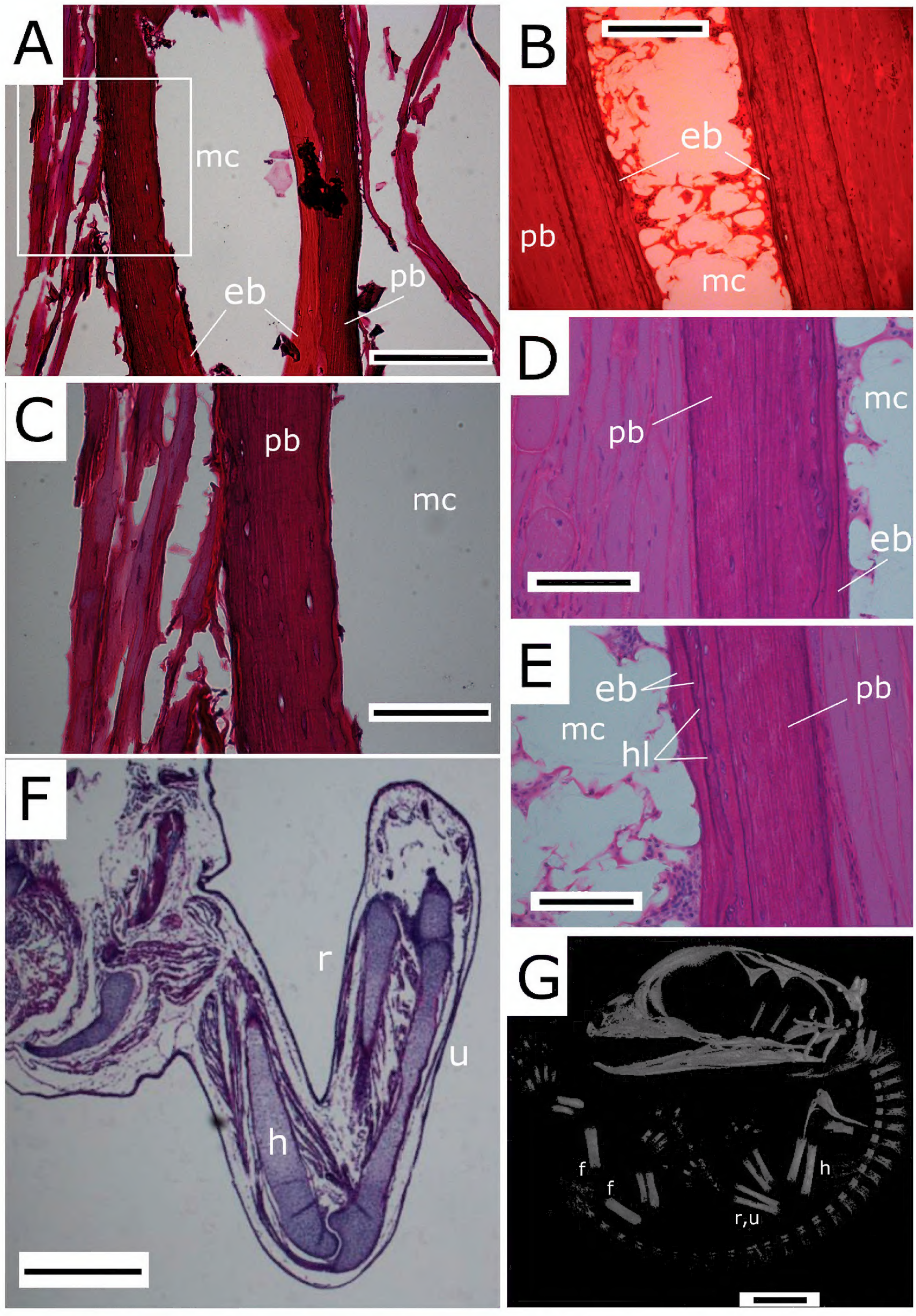

Figure 6. Bone histology of *Hemidactylus* long bones. Adult specimen CA2017_001 (cross section no. H63_FR_B5; **A, C**), ZMB 87078 (cross section no. A12_FL_6b, one year old, SVL 47 mm; **B, D, E**), and developmental stage I specimen CA2017_015 **(F)** and CA2017_014 **(G)**. **(A–E)** Longitudinal sections (HE staining) of the humeral shaft showing a clear pattern of alternating bone lamellae in the periosteal cortex and remodeling in the endosteal region. **(C)** Close-up of boxed area in **(A)**. **(D, E)** Magnification of cortical bone of similar areas in **(B)**. **(F, G)** Onset of ossification in individuals, 25 days before hatching, as seen in histological sections **(F)** and μCT scans **(G)**. Abbreviations: **eb** – endosteal bone; **f** – femur; **h** – humerus; **hl** – Howship lacunae; **mc** – medullary cavity; **pb** – periosteal bone; **r** – radius; **u** – ulna. Scale bars in **(A, B)** equal 200 μm, in **(C–E)** 100 μm, in **(F)** 500 μm, and 1 mm in **(G)**.

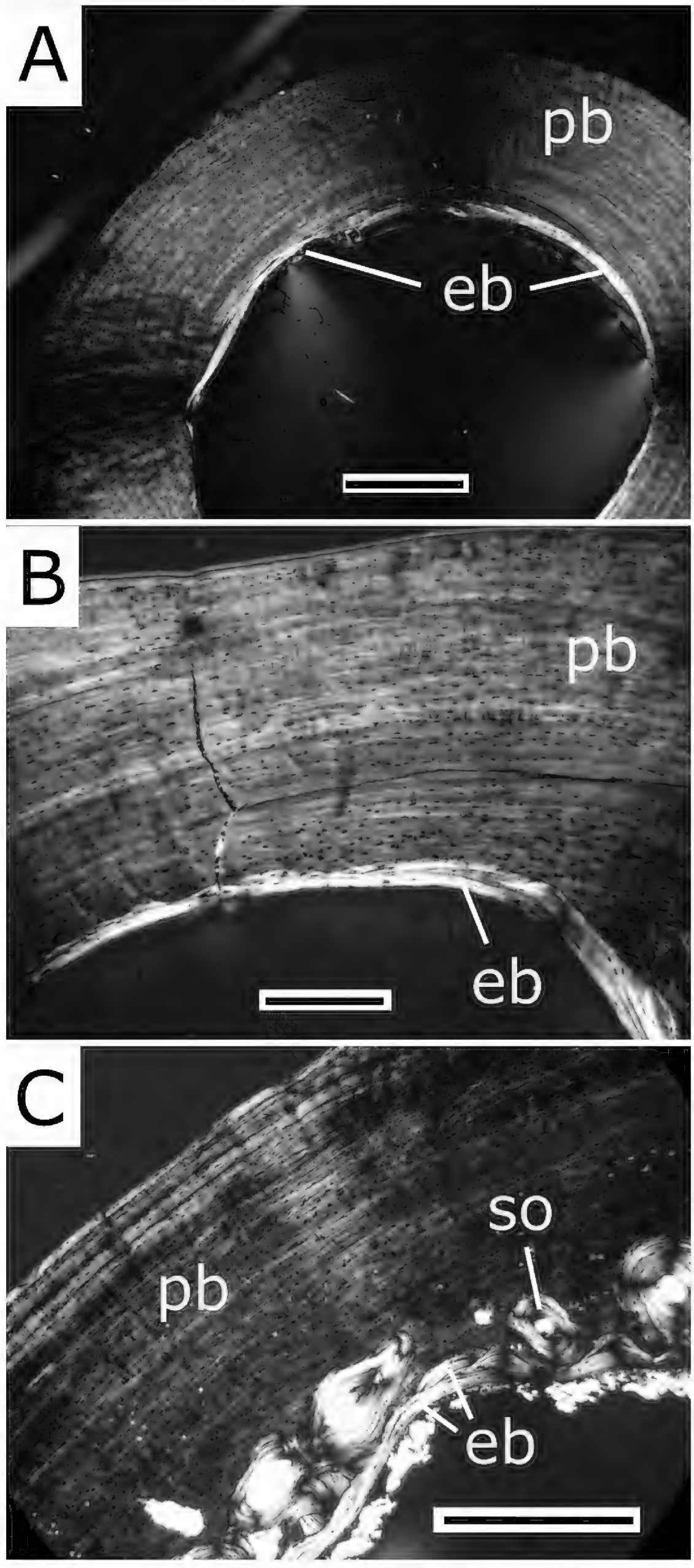

Figure 7. Lamellar bone histology and endosteal remodeling in other squamate lizards. **(A)** Cross section of an *Iguana iguana* femur (AC1896 288). **(B)** Cross section of a *Varanus timorensis* femur (MK52920). **(C)** Cross section of *Tupinambis teguixin* femur (MK53531). All images were taken under cross polarized light. Note the cross cutting relations in the endosteal bone of *V. timorensis* and *Tupinambis*. Also note the more extensive layer of remodeling with secondary osteons in the innermost cortex of *Tupinambis*. Abbreviations: **eb** – endosteal bone; **pb** – periosteal bone; **so** – secondary osteon. Scale bar in **(A)** equals 1 mm, in **(B)** 250 μm, and in **(C)** 500 μm.

Discussion and conlusions

Comparative embryology

The *in-ovo* development of the gecko *Hemidactylus* was defined into twelve stages post-oviposition based on morphological embryonic characters (Figs 2, 3). In contrast to other staging tables, somite formation is not taken into account as they are not clearly identifiable (Hamburger and Hamilton 1951, Muthukkaruppan et al. 1970, Theiler 1989, Sanger et al. 2008). The comparisons of days post-oviposition proved to be a poor indicator of actual development of the embryo (Tab. 1), which we attribute to variations in oviposition timing between females and/or to fluctuation in temperature (26-28°C) in the breeding room. Such discrepancy is not unusual considering the poikilothermic physiology of *Hemidactylus*; shifts in temperature are known to have effects on the developmental age of individuals (Atkinson 1994, Andrews 2004, Goodman 2008, Dayananda et al. 2017). A similar range was also monitored in *Eublepharis macularius* (Wise et al. 2009), *Nothobachia ablephara* and *Calyptommatus sinebrachiatus* (Roscito and Rodrigues 2012). Instead, our study groups erected stages based on morphological events regarding the ear, eye, head, heart, limbs, fronto-nasal process, pharyngeal arches, skin, and thorax development (Figs 2, 3; Tabs 1, 3). Since limb morphogenesis is an often used and a very informative criterion in vertebrate developmental biology, it is also a focus in this study. We not only generated a framework in which to communicate the development of *Hemidactylus*, but we also made direct comparisons with other staging tables available for a diverse range of squamate species (Tab. 3), thus allowing comparative heterochronic studies. In fact, in squamates, the differential timing of fore- and hind limb is rather synchronous (Bininda-Emonds et al. 2007). Interestingly, this is also the case in *Hemidactylus,* which shows no heterochrony in limb development (Tab. 1), in contrast to other gekkotan taxa in which forelimb development is slightly advanced (Noro et al. 2009, Wise et al. 2009). Furthermore, in *Paroedura*, which has a comparable

Table 3. Comparison of squamate staging tables. Differing stages were horizontally aligned based on key characters. Comparing different staging tables allows for the study of heterochrony within squamates, here including geckos, lacertids and iguanians. Focused on limb development, darkening shades of gray indicate (i) both limb buds present after oviposition, (ii) interdigital tissue starts retreating, (iii) develops claws on all 5 digits, (iv) first sign of scales on limbs, and (v) limbs fully developed apart from size. Abbreviations: dpo – days post-oviposition; S, St – embryonic stage.

This study	Noro et al. (2009)	Khannoon (2015)	Wise et al. (2009)	Roscito and Rodrigues (2012)	Roscito and Rodrigues (2012)	Py-Daniel et al. (2017)	Sanger et al. (2008)	Muthukkarruppan et al. (1970)
Hemidactylus sp.	*Paroedura pictus*	*Tarentola annularis*	*Eublepharis macularius*	*Nothobachia ablephara*	*Calyptommatus sinebrachiatus*	*Tropidurus torquatus*	*Anolis sagrei*	*Calotes versicolor*
	0 dpo							Stage 27
	1 dpo							Stage 28
Stage A	2 dpo		St 28		St 1			
Stage B	3-4-5 dpo		St 29	St 1	St 2-3	St 28	3	Stage 29
	6-7 dpo	S29		St 2		St 29	4-5	
Stage C	8-9-10 dpo		St 30		St 4	St 30	6	Stage 30
		S30						
	12 dpo			St 3				Stage 31
Stage D	14 dpo		St 31	St 4	St 5	St 31		
		S31		St 5		St 32		
					St 6			Stage 32
	16 dpo		St 32					
Stage E	18 dpo	S32	St 33	St 6	St 7	St 33-34	7-8	Stage 33
Stage F	20-22 dpo	S33	St 34	St 7	St 8	St 35	9	Stage 34
				St 8	St 9-10			
Stage G	24 dpo	S34		St 9	St 11	St 36	10	Stage 35
	26 dpo		St 35				11	
Stage H	28 dpo	S35	St 36			St 37		Stage 36
Stage I	30 dpo	S36	St 37			St 38	12-13-14	
								Stage 37
								Stage 38
Stage J	35 dpo	S37	St 38			St 39	15-16-17	Stage 39
			St 39					
		S38	St 40					Stage 40
Stage K	40-45-50 dpo	S39	St 41		St 12	St 40	18	Stage 41
Stage L	55-60 dpo		St 42			St 41-42	19	Stage 42

developmental period, limb budding starts at the third day of oviposition (Noro et al. 2009). In contrast, we observe that in *Hemidactylus*, limb budding does not start as early as stage B (Fig. 2, Tab. 1). Later in development, Noro et al. (2009) identify a pattern of heterochrony in the limbs of *Paroedura*, which they attribute to the development of the digits in the gekkotan clade. However, findings of this study do not support this assumption (Figs 2, 3). Instead, we found interspecific variation during limb development within eight squamate species including geckos, lacertids, and iguanians: (i) concerning limb bud formation after oviposition, (ii) retraction of the interdigital tissue, (iii) claw development on the ultimate phalanges, (iv) scale formation on the limbs, and (v) termination of limb development (Tab. 3). Among geckos, for example, scale formation on the limbs starts at stage J and 35 dpo in *Hemidactylus* and *Paroedura*, respectively, whereas in *Tarentola* and *Eublepharis*, it is developed at an earlier stage (S35 and St 37, respectively).

Long bone histomorphometrics

Bone histology shows rapid accretion and endosteal remodeling of lamellar bone in the long bone cortices at later phases in ontogeny. The lamellar bone formation rate is similar to rates seen in the nearly avascular fibulae of wild *Varanus niloticus* (de Buffrénil and Castanet 2000), suggesting that absolute matrix production rate could be similar in different squamates. The intense remodeling in adult *Hemidactylus* indicates a dynamic balance of cortical bone thickness during growth. Interestingly, in contrast to *Hemidactylus*, *Iguana*, and *Varanus timorensis*, the *Tupinambis* (Fig. 7) in our study also produces secondary osteons, and generally experiences more advanced remodeling. This difference may be the result of the combination of the relatively large size and foraging behavioral ecology of *Tupinambis*. The studied *Hemicactylus* and *V. timorensis* also typically forage for food, but they retain relatively small body sizes, and their lacuno-canalicular networks may provide enough flux to maintain a healthy bone homeostasis without the need for additional blood vessels inside the bony cortex.

Eco-specializations of the limbs of Hemidactylus

Our detailed analysis of ecomorphological specializations in the limbs of *Hemidactylus* also reveal that, in contrast to earlier observations (Russell and Bauer 1988), paraphalanges are bony in the adult, as revealed by μCT (Figs 3, 4). However, these ossify only after hatching, as shown by μCT scanning and azan staining (Figs 4, 5). Furthermore, data from the μCT indicate that more paraphalanges in various different shapes are present in *Hemidactylus* (Fig. 4), when compared to other gekkotans (Gamble et al. 2012). These structures have been suggested to aid in the support of the scansors (Russell and Bauer 1988, Gamble et al. 2012). In fact, they evolved also multiple times independently in geckos, alongside adhesive toepads (Gamble et al. 2012). Paraphalanges have been suggested to represent sesamoid bones (Russell and Bauer 1988, Gamble et al. 2012). Sesamoids are neomorphic ossifications present in tendons and/or ligaments, located near joints. They are often mistaken for accessory ossicles because both share various imaging characteristics (Nwawka et al. 2013). However, we agree with their previous identification as paraphalanges, because their existence correlates with the modified tendons and muscles controlling the scansors (Russell and Bauer 1988, Gamble et al. 2012). Among Squamata, a variety of different sesamoid bones are present in the hands and feet (Fontanarrosa and Abdala 2016, Regnault et al. 2016). In fact, phalangeal sesamoids, located dorsally on the penultimate phalanges, are ancestral to all Lepidosauria (squamates and rhynchocephalians), whereas metacarpal sesamoids likely evolved only later within squamates (Regnault et al. 2016). Penultimate phalangeal sesamoids are, in fact, present in most squamates (Regnault et al. 2016). Metacarpal and metatarsal sesamoids are of variable occurrence in Gekkota (Regnault et al. 2016). Although some sesamoids have been linked to lifestyle, functional interpretations are to be inferred with caution (Fontanarrosa and Abdala 2016, Regnault et al. 2016). In humans, e.g., sesamoids likely result from an interplay of intrinsic genetic factors and phylogeny, and extrinsic mechanobiological factors (Sarin et al. 1999).

Reduced phalanges ossify at the same time schedule as the other phalangeal elements in *Hemidactylus* (Figs 3, 4), but their ecological relevance is yet to be determined in this species. This trait is also found in non-related and ecologically different fossil synapsids, such as *Biarmosuchus*, *Titanophoneus*, *Lycaenops*, *Thrinaxodo*n, and even the mammaliaform *Docofossor* (Hopson 1995, Luo et al. 2015). However, phalanx number varies widely in non-mammalian tetrapods (Richardson and Chipman 2003). Hopson (1995) suggested that these reduced disc-like structures were eventually lost. Gamble et al. (2012), on the other hand, linked phalanx reduction with the evolution of adhesive toepads. Furthermore, Russell (1977) suggested that the reduced phalanx is used to raise the penultimate phalanx, thereby altering the angle of the claw relative to the substrate for a more beneficial grip. Phalanx variation has been developmentally associated with either heterochronic shifts (Richardson and Oelschläger 2002), or the involvement of mutations in expression patterns and molecular pathways of BMPs and other transcription factors (Cooper et al. 2014, Luo et al. 2015). Studying the latter in *Hemidactylus* remains an avenue for future research. This study provides the morphological framework essential for the study of such kinds of ecological traits from a molecular perspective, that is, by means of gene expression and transcriptome analyses.

Author contributions

CB designed the study. CB and WvdV collected gecko embryos. WdV carried out experiments in the morphology & histology lab. CB compiled μCT datasets. KS carried

out bone histology experiments. CB, KS, and WvdV analyzed data. NDP provided reagents and lab facilities for immunohistochemical analyses, and commented on an earlier version of the manuscript. CB, KS, and WvdV wrote the manuscript. All authors approved the final version.

Acknowledgements

Johannes Müller (Berlin) provided the parental *Hemidactylus* generation and helped with animal husbandry; we thank him also for discussion. Annett Billepp and Petra Grimm (Berlin) are thanked for animal care-taking. We thank Julia Eymann (Helsinki) for help with immunohistochemical analyses. We thank Jutta Zeller (Berlin) for help with and preparation of histological sections and staining. Kristin Mahlow (Berlin) is thanked for help with μCT scanning. Frank Tillack (Berlin) kindly helped with taking photos of live animals. We furthermore thank Vivian de Buffrénil (Paris) for access to comparative material of *Varanus timorensis*, *Tupinambis teguixin*, and *Iguana iguana* at the histology library of the Musée d'Histoire Naturelle. We also thank Brandon Kilbourne (Berlin) for language editing of an earlier version of the manuscript. We acknowledge critical and helpful comments by Torsten Scheyer (Zurich) and Johannes Penner (Freiburg). CB and WvdV were funded by the German Research Foundation (DFG, BI 1750/3-1 to CB); KS was funded by a postdoctoral mandate of the Research Foundation Flanders (FWO).

References

Andrews RM (2004) Patterns of embryonic development. In: Deeming DC (Ed.) Reptilian Incubation: Environment, Evolution And Behaviour. Nottingham University Press, Nottingham. 75–102.

Arnold EN, Poinar G (2008) A 100 million year old gecko with sophisticated adhesive toe pads preserved in amber from Myanmar. Natural History 1847: 6–68.

Atkinson D (1994) Temperature and organism size - a biological law for ectotherms? Advances in Ecological Research 25: 1–58. https://doi.org/10.1016/S0065-2504(08)60212-3

Autumn K, Sitti M, Liang YA Peattie AM, Hansen WR, Sponberg S, Kenny TW, Fearing R, Israelachvili JN, Full RJ (2002) Evidence for van der Waals adhesion in gecko setae. Proceedings of the National Academy of Sciences of the United States of America 99: 12252–12256. https://doi.org/10.1073/pnas.192252799

Bininda-Emonds O, Cardillo M, Jones KE, MacPhee RDE, Beck RMD, Grenyer R, Price SA, Vos RA, Gittleman JL, Purvis A (2007) The delayed rise of present-day mammals. Nature 446: 507–512. https://doi.org/10.1038/nature05634

de Buffrenil V, Castanet J (2000) Age estimation by skeletochronology in the Nile monitor (*Varanus niloticus*), a highly exploited species. Journal of Herpetology 34: 414–424. https://doi.org/10.2307/1565365

Carranza S, Arnold EN (2006) Systematics, biogeography, and evolution of *Hemidactylus* geckos (Reptilia: Gekkonidae) elucidated using mitochondrial DNA sequences. Molecular Phylogenetics and Evolution 38: 531–545. https://doi.org/10.1016/j.ympev.2005.07.012

Cooper KL, Sears KE, Uygur A, Maier J, Baczkowski KS, Brosnahan M, Antczak D, Skidmore JA, Tabin CJ (2014) Patterning and post-patterning modes of evolutionary digit loss in mammals. Nature 511: 41–45. https://doi.org/10.1038/nature13496

Dayananda B, Penfold S, Webb JK (2017) The effects of incubation temperature on locomotor performance, growth and survival in hatchling velvet geckos. Journal of Zoology. https://doi.org/10.1111/jzo.12460

Fontanarrosa G, Abdala V (2016) Bone indicators of grasping hands in lizards. PeerJ 4: e1978. https://doi.org/10.7717/peerj.1978

Gamble T, Greenbaum E, Jackman TR, Russell AP, Bauer AM (2012) Repeated origin and loss of adhesive toepads in geckos. PLoS ONE 7: e39429. https://doi.org/10.1371/journal.pone.0039429

Gilbert F, Epel D (2009) Ecological developmental biology: integrating epigenetics, medicine and evolution. Sinauer Associates Inc, Sunderland, Massachusetts, 480 pp.

Goodman RM (2008) Latent effects of egg incubation temperature on growth in the lizard *Anolis carolinensis*. Journal of Experimental Zoology Part A: Ecological Genetics and Physiology 309: 525–533. https://doi.org/10.1002/jez.483

Hamburger V, Hamilton H (1951) A series of normal stages in the development of the chick embryo. Journal of Morphology 88: 231–272. https://doi.org/10.1002/jmor.1050880104

Hopson JA (1995) Patterns of evolution in the manus and pes of non-mammalian therapsids. Journal of Vertebrate Paleontology 15: 615–639. https://doi.org/10.1080/02724634.1995.10011252

Hugi J, Hutchinson MN, Koyabu D, Sánchez-Villagra MR (2012) Heterochronic shifts in the ossification sequences of surface-and subsurface-dwelling skinks are correlated with the degree of limb reduction. Zoology 115: 188–198. https://doi.org/10.1016/j.zool.2011.10.003

Khannoon ER (2015) Developmental stages of the climbing gecko *Tarentola annularis* with special reference to the claws, pad lamellae, and subdigital setae. Journal of Experimental Zoology Part B Molecular and Developmental Evolution 324: 450–464. https://doi.org/10.1002/jez.b.22630

Losos JB, Hillis DM, Greene HW (2012) Who speaks with a forked tongue? Science 338: 1428–1429. https://doi.org/10.1126/science.1232455

Luo Z-X, Meng Q, Ji Q, Zhang Y-G, Neander AI (2015) Evolutionary development in basal mammaliaforms as revealed by a docodontan. Science 347: 760–764. https://doi.org/10.1126/science.1260880

Millinkovitch MC, Tzika A (2007) Escaping the mouse trap: The selection of new evo-devo model species. Journal of Experimental Zoology 308B: 337–346. https://doi.org/10.1002/jez.b.21180

Muthukkaruppan V, Kanakambika P, Manickavel V, Veeraraghaven K (1970) Analysis of the development of the lizard, *Calotes versicolor*. Journal of Morphology 130: 479–490. https://doi.org/10.1002/jmor.1051300407

Noro M, Uejima A, Abe G, Manabe M, Tamura K (2009) Normal developmental stages of the Madagascar Ground Gecko *Paroedura pictus* with special reference to limb morphogenesis. Developmental Dynamics 238: 100–109. https://doi.org/10.1002/dvdy.21828

Nwawka OK, Hayashi D, Diaz LE, Goud AR, Arndt III WF, Roemer FW, Malguria N, Guermazi A (2013) Sesamoids and accessory ossicles of the foot: anatomical variability and related pathology. Insights Imaging 4: 581–593. https://doi.org/10.1007/s13244-013-0277-1

Pianka ER, Sweet SS (2005) Integrative biology of sticky feet in geckos. BioEssays 27: 647–652. https://doi.org/10.1002/bies.20237

Py-Daniel R, Kennedy Soares De-Lima A, Campos Lima F, Pic-Taylor A, Rodrigues Pires Junior O, Sebben A (2017) A staging table of

post-ovipositional development for the South American collared lizard *Tropidurus torquatus* (Squamata: Tropiduridae). The Anatomical Record 300: 277–290. https://doi.org/10.1002/ar.23500

Pyron RA, Burbrink FT, Wiens JJ (2013) A phylogeny and revised classification of Squamata, including 4161 species of lizards and snakes. BMC evolutionary biology 13: 93. https://doi.org/10.1186/1471-2148-13-93

Rasband WS (1997) ImageJ. US National Institutes of Health, Bethesda, MD.

Regnault S, Jones MEH, Pitsillides AA, Hutchinson JR (2016) Anatomy, morphology and evolution of the patella in squamate lizards and tuatara (*Sphenodon punctatus*). Journal of Anatomy 228: 864–876. https://doi.org/10.1111/joa.12435

Richardson MK, Oelschläger HHA (2002) Time, pattern, and heterochrony: a study on hyperphalangy in the dolphin embryo flipper. Evolution and Development 4: 435–444. https://doi.org/10.1046/j.1525-142X.2002.02032.x

Richardson MK, Chipman AD (2003) Developmental constraints in a comparative framework: a test case using variations in phalanx number during amniote evolution. Journal of Experimental Zoology Part B Molecular and Developmental Evolution 296: 8–22. https://doi.org/10.1002/jez.b.13

Roscito JG, Rodrigues MT (2012) Embryonic development of the fossorial gymnophthalmid lizards *Nothobachia ablephara* and *Calyptommatus sinebrachiatus*. Zoology 115: 302–318. https://doi.org/10.1016/j.zool.2012.03.003

Ruibal R, Ernst V (1965) The structure of the digital setae of lizards. Journal of Morphology 117: 271–293. https://doi.org/10.1002/jmor.1051170302

Russell AP (1975) A contribution to the functional analysis of the foot of the Tokay gecko, *Gekko gecko*. Journal of Zoology 176: 437–476. https://doi.org/10.1111/j.1469-7998.1975.tb03215.x

Russell AP (1977) The phalangeal formula of *Hemidactylus* Oken: A correction and a functional explanation. Anatomia, Histologia, Embryologia 6: 332–338. https://doi.org/10.1111/j.1439-0264.1977.tb00443.x

Russell AP (2002) Integrative functional morphology of the gekkotan adhesive system (Reptilia: Gekkota). Integrative and Comparative Biology 42: 1154–1163. https://doi.org/10.1093/icb/42.6.1154

Russell AP, Bauer AM (1988) Paraphalangeal elements of gekkonid lizards: a comparative survey. Journal of Morphology 197: 221–240. https://doi.org/10.1002/jmor.1051970208

Sanger TJ, Losos JB, Gibson-Brown JJ (2008) A developmental staging series for the lizard genus *Anolis*: a new system for the integration of evolution development, and ecology. Journal of Morphology 296: 129–137. https://doi.org/10.1002/jmor.10563

Sanger TJ (2012) The emergence of squamates as model systems for integrative biology. Evolution and Development 14: 231–233. https://doi.org/10.1111/j.1525-142X.2012.00541.x

Sarin VK, Erickson GM, Giori NJ, Bergmann AG, Carter DR (1999) Coincident development of sesamoid bones and clues to their evolution. The Anatomical Record 257: 174–180. https://doi.org/10.1002/(SICI)1097-0185(19991015)257:5<174::AID-AR6>3.0.CO;2-O

Shapiro MD (2002) Developmental morphology of limb reduction in *Hemiergis* (Squamata: Scincidae): chondrogenesis, osteogenesis, and heterochrony. Journal of Morphology 254: 211–231. https://doi.org/10.1002/jmor.10027

Theiler K (1989) The House Mouse: Atlas Of Embryonic Development. Springer-Verlag, New York Inc, New York.

Vickaryous MK, Olson MW (2007) Sesamoids and ossicles in the appendicular skeleton. In: Hall BK (Ed.) Fins into Limbs: Evolution, development, and transformation. The University of Chicago Press, Chicago, 323–341.

Wellborn V (1933) Vergleichende osteologische Untersuchungen an Geckoniden, Eublephariden und Uroplatiden. Sitzung der Gesellschaft Naturfreunde, Berlin.

Wiens JJ, Hutter CR., Mulcahy, D. G., Noonan BP, Townsend TM, Sites Jr JW, Reeder TW (2012) Resolving the phylogeny of lizards and snakes (Squamata) with extensive sampling of genes and species. Biology Letters 8: 1043–1046. https://doi.org/10.1098/rsbl.2012.0703

Wise PAD, Vickaryous MK, Russell AP (2009) An embryonic staging table for in ovo development of *Eublepharis macularius*, the leopard gecko. The Anatomical Record: Advances in Integrative Anatomy and Evolutionary Biology 292: 1198–1212. https://doi.org/10.1002/ar.20945

Supplementary material 1

SOM Table

Authors: Wessel van der Vos, Koen Stein, Nicolas Di-Poï, Constanze Bickelmann

Data type: Adobe PDF file

Explanation note: μCT scanning details for specimens used in this study and depicted in Figures 2, 4-6.

Link: https://doi.org/10.3897/zse.94.22289.suppl1